ISSN: **3107-6513**

Assessment of Climate-Related Bluetongue Virus in Ill-Bled Sheep Carcasses from Egyptian Abattoirs

Ashraf Kassem[1], Marwa Khattab[1], Elshaimaa Ismael[2], Aya Yassin[3], Dalia Hamza[4], Ahmed Osman[1]

1 Department of Pathology, Faculty of Veterinary Medicine, Cairo University, Giza, 12211, Egypt.

2 Department of Veterinary Hygiene and Management, Faculty of Veterinary Medicine, Cairo University, Giza, 12211, Egypt.

3 Department of Biochemistry and Molecular Biology, Faculty of Veterinary Medicine, Cairo University, Giza, 12211, Egypt.

4 Department of Zoonoses, Faculty of Veterinary Medicine, Cairo University, Giza, 12211, Egypt.

1vetashrafkassem567@gmail.com, 2marwakhattab@cu.edu.eg, 3ahosman2007@cu.edu.eg

***Abstract*—** The emergence of Bluetongue virus (BTV) in Egypt, along with its association with ill-bled condemned sheep carcasses, highlights the growing effects of environmental change on the epidemiology of vector-borne diseases. Rising temperatures facilitate the development of vector habitats, increasing the risk of transmission and potentially leading to severe outcomes such as ill-bleeding and the condemnation of entire carcasses. A detailed case-series study was conducted at the Al-Basatin automated slaughterhouse and 15 May Semi-Automated Abattoir in Cairo, spanning from June 2024 to May 2025, involving 100 sheep carcasses that were entirely condemned. A total of nineteen ill-bled carcasses underwent molecular and biochemical analysis for the detection of BTV using RT-PCR, as well as for oxidative stress biomarkers including total antioxidant capacity (TAC), malondialdehyde (MDA), and reduced glutathione (GSH). In addition, the expression of genes related to heat stress, including heat shock protein 70 KDa protein 1A (HSP70) and bradykinin receptor B1 (BDKRB1), was assessed. Furthermore, key signaling molecules involved in bluetongue virus (BTV)–induced immune responses, namely interferon regulatory factor 3 (IRF3) and signal transducer and activator of transcription 2 (STAT2), were analyzed. The BTV-positive ill-bled animals were subjected to histopathological examination and immunohistochemistry for cyclooxygenase-2 (COX-2) and inducible Nitric Oxide Synthase (iNOS). Additionally, Meteorological records from national climate monitoring agencies were also used to estimate the Temperature–Humidity Index for sheep (THI_{sheep}) on the dates of sample collection. Molecular testing has verified the presence of BTV RNA in 63.2% of the examined heart and lung samples. The gross and histopathological observations indicated degeneration and necrosis in parenchymatous organs such as the heart, liver, kidney, and lung, in all ill-bled condemned sheep carcasses, which were consistent with BTV infection. This was further supported by the elevated expression of COX-2 and iNOS. The ill-bleeding observed in sheep carcasses demonstrated a strong and statistically significant correlation with the level of heat stress, as evaluated by THI (p = 0.023). Biochemical analyses showed increased levels of MDA, alongside decreased concentrations of TAC, GSH with variable levels of HSP70, BDKRB1, IRF3 and STAT2, in heart and lung tissues. Indicating heightened oxidative stress coupled with reduced antioxidant capacity under conditions of heat stress. Our current findings highlight the impact of climate extremes in animal disease dynamics and indicating a substantial correlation between heat stress and ill-bleeding in sheep, mediated by BTV infection and oxidative stress.

Keywords*— *Climate change, Bluetongue virus, Ill-bleeding, Pathology, THI, Egypt

Graphical abstract

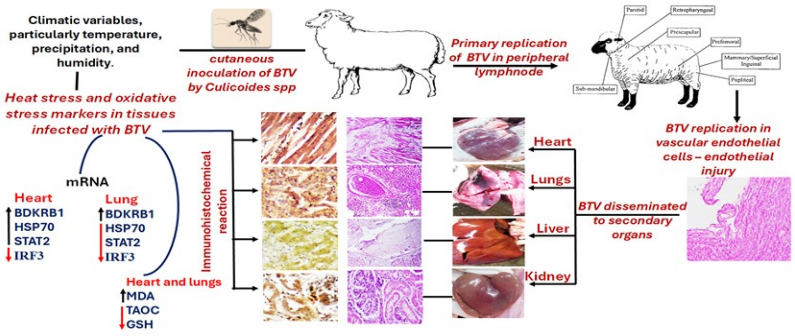

I. INTRODUCTION

Climate change represents a significant global issue that has extensive repercussions for both human and animal health, agricultural practices, and the stability of ecosystems. These alterations pose a threat to the advancement of various United Nations Sustainable Development Goals (SDGs), notably Goal 2 (Zero Hunger), Goal 3 (Good Health and Well-being), Goal 13 (Climate Action), and Goal 15 (Life on Land) [1].

Sheep, as small ruminants that have adapted to a variety of ecological environments, exhibit a marked susceptibility to environmental changes, particularly elevated ambient temperatures, shifts in precipitation patterns, and the growing occurrence of extreme climatic events [2]. These climatic shifts impose both direct and indirect influences on the physiology and production systems of sheep [3].

Sheep, which are essential to rural economies and food systems, are especially susceptible to heat stress due to their dependence on surrounding environmental conditions. As homeothermic creatures, sheep strive to maintain a consistent core body temperature (38.3 - 39.9°C); however, when ambient temperatures surpass their thermoneutral zone (5 - 25°C), particularly during late spring and summer, they activate thermoregulatory responses such as increased respiration and peripheral vasodilation to avert hyperthermia [4,5]. If these mechanisms fail, core temperatures may rise above 40.5°C, resulting in heat stress that adversely impacts immunity, feed efficiency, and reproductive capabilities [6].

Sheep are among the most susceptible hosts to (BTV), a vector-borne viral illness of ruminants with substantial economic significance [7]. Biting midges of the Culicoides species are the main way that the (BTV) is transmitted [8]. The epidemiology of (BTV) is heavily influenced by climatic factors, particularly temperature, precipitation, and humidity, which determine the distribution, population density, and vectorial capacity of Culicoides populations [9]. Elevated ambient temperatures hasten viral replication within the vector, reduce the extrinsic incubation period, and prolong seasonal transmission periods, thereby heightening the probability of outbreaks [10].

In sheep, infection with (BTV) can lead to acute and occasionally fatal disease, which is characterized by fever, oedema, mucosal erosions, respiratory distress, and diminished productivity [11]. The severity of clinical manifestations is influenced by viral serotype, host genetics, and immune status, but is also affected by environmental stressors [12]. Heat stress, caused by elevated ambient temperatures, has been demonstrated to impair immune function in small ruminants, making these animals more susceptible to viral infections and worsening disease severity [13]. The pathogenesis of (BTV) is closely linked to its affinity for vascular endothelial cells, resulting in extensive vascular damage, increased permeability, and compromised haemostasis [14].

This vascular injury is the primary mechanism behind the distinctive clinical syndrome of “ill-bleeding” seen in sheep, which is exhibited as petechiae, ecchymoses, mucosal haemorrhages, and cyanosis of the tongue [15]. The combination of endothelial disruption, inflammatory cytokine release, and coagulopathic disturbances leads to fragile blood vessels and uncontrolled bleeding [16]. One important pathogenic component linked to the development of viral infections, including BTV, is oxidative stress [17]. Excessive reactive oxygen species (ROS) are produced by viral replication and host inflammatory reactions, which lead to DNA damage, lipid peroxidation, and protein oxidation [18]. Oxidative stress is linked to endothelial dysfunction, vascular damage, and an increase of inflammatory processes that cause clinical signs in sheep infected with BTV [19]. Simultaneously, heat stress linked to changing climatic conditions further disrupts redox homeostasis, exacerbating oxidative damage and diminishing the effectiveness of antioxidant defence mechanisms [20]. The interplay between viral infection, oxidative stress, and climatic factors, therefore, represents a critical axis in the progression and outcome of BT in sheep.

Despite the growing recognition of the interconnections among climate, health, and ecosystems, a considerable gap persists in comprehending the interactions between heat stress, oxidative damage, vector-borne diseases, and ill-bleeding in sheep. This case series seeks to address that gap by documenting the clinical and pathological characteristics of heat stress and BTV-associated ill-bleeding in sheep within Egyptian slaughterhouses. Furthermore, the study highlights the significance of abattoir-based surveillance as a proactive warning mechanism for emerging animal diseases, which is an essential measure towards fulfilling SDG 15 (Life on Land) through enhanced animal health, the preservation of biodiversity, and the sustainable management of livestock.

II. MATERIALS AND METHODS

A. Study animals and inclusion criteria

This descriptive case series involved 100 ossimi sheep carcasses that were entirely condemned during routine meat inspections at the Al-Basatin automated slaughterhouse and 15 May Semi-Automated Abattoir in Cairo, Egypt, spanning from June 2024 to May 2025. All cases that were condemned during this timeframe were included in a consecutive manner, without any random selection process. The sheep, ranging in age from 1 to 3 years and comprising both sexes, were representative of the typical animals processed at this facility. Comprehensive meat inspections were performed on all carcasses, and 19 carcasses (16 ram and 3 ewe) exhibited clear signs of ill-bleeding [21], were chosen for further examination. The study protocol was approved by the Institutional Animal Care and Use Committee (IACUC) of the Faculty of Veterinary Medicine, Cairo University (Approval number: Vet CU11052025115).

B. Sample size justification

The sample size was determined by case availability rather than a prior calculation, as the study was designed as a descriptive case series including all ill-bleeding cases identified throughout the study period [22]. The final number of cases (n = 19) represents the entire population of ill-bled sheep carcasses detected among all condemned cases during the surveillance period, ensuring complete case capture and minimising selection bias.

C. Pathological investigation

During routine meat inspections, 19 of the 100 condemned carcasses showed evidence of ill-bleeding. Detailed gross examination was performed on these carcasses and their major organs, including the heart, lungs, liver, kidneys, aorta, and pulmonary artery, to identify lesions due to impaired exsanguination [21].

D. Samples collection and preparation

Heart, lungs, liver, and kidneys of ill bled sheep carcasses tissue samples were collected then divided into two distinct parts. The initial portion was preserved in 10% neutral-buffered formalin for histopathology and immunohistochemistry evaluations. The subsequent part was frozen and then processed into tissue homogenates for molecular and biochemical investigations [23]. A total of 19 ill bled carcasses were examined for bluetongue virus (BTV) infection utilizing PCR techniques for heart and lung samples. The cases that tested positive for BTV were then further analysed for oxidative stress markers and gene expression.

E. Molecular detection of Bluetongue virus (BTV) by RT-PCR

The QIAamp Viral RNA Mini Kit (Qiagen, Germany) was used to extract viral RNA from heart and lung tissue samples in accordance with the manufacturer's instructions.

For the molecular detection of (BTV), a two-step RT-PCR was performed. In the first step, reverse transcription was carried out using the RevertAid First Strand cDNA Synthesis Kit (Thermo Fisher, USA). A total of 20 µL of nuclease-free water was added to the reaction mixture, which included 5 µL extracted RNA, 1 µL Oligo(dT) primers or random hexamers, 4 µL of 5× Reverse Transcription Buffer, 1 µL of Ribolock RNase inhibitor (20 U/µL), 2 µL of dNTP mix (10 mM each), and 1 µL of RevertAid Reverse Transcriptase (200 U/µL). After primer annealing for five minutes at 25°C, reverse transcription for sixty minutes at 42°C, and enzyme inactivation for five minutes at 70°C, the reaction was incubated.

The VP7 protein gene was the target of PCR amplification in the second step, which was carried out using the following primers: Forward (5'-TCGCTGCCATGCTATCCG-3') and Reverse (5'-CGTACGATGCGAATGCAG-3'). A total of 20 µL of nuclease-free water, 2 µL of cDNA, 10 µL of 2× PCR Master Mix (Thermo Fisher, USA), 1 µL of forward primer (10 µM), and 1 µL of reverse primer (10 µM) made up the reaction mixture. The PCR cycling conditions comprised a 5-minute initial denaturation at 95°C, 35 cycles of denaturation at 94°C for 30 seconds, annealing at 52°C for 30 seconds, and extension at 72°C for 30 seconds, and a final extension at 72°C for 10 minutes. Ethidium bromide staining was used to visualize the PCR products at amplicon size 251 bp after they were examined using 1.5% agarose gel electrophoresis.

F. Histopathological examination

After being preserved in 10% neutral buffered formalin, tissue samples from the heart, lungs, liver, kidneys, aorta, and pulmonary artery were processed using the paraffin embedding technique. Using a rotary microtome, 4 µm thick sections were prepared, stained with haematoxylin and eosin, and examined under a light digital microscope (Olympus xc30, Tokyo, Japan) [24]. The Prussian blue staining method was performed to detect iron deposition [25].

G. Immunohistochemical examination

Primary antibodies against COX-2 (sc-19999) and iNOS (GB12086) were used after deparaffinization, rehydration, and antigen retrieval using citrate buffer (pH 6). As directed by the manufacturer (BIO SB, mouse/rabbit HRP immunodetector detection system, USA), a biotinylated secondary antibody and horseradish peroxidase (HRP)-labeled avidin were utilized. Diaminobenzidine was utilized as a substrate and hematoxylin as a counterstain [26]. Positive control slides were stained with antibodies unique to the target species, whereas negative control slides were only stained with secondary antibodies (not primary antibodies). An internal positive anatomical control determined that COX-2 and iNOS expressions were positive.

H. Assessment of oxidative stress biomarkers

Heart and lung tissue samples were collected and rinsed with ice-cold phosphate-buffered saline (PBS) to remove blood. The tissues were then homogenized in cold PBS (1:10 w/v). Homogenates were centrifuged at 10,000 × g for 10 min at 4°C, and the supernatants were collected and stored at -20°C for further analysis. The supernatant was used for the measurement of total antioxidant capacity (TAC) reduced glutathione (GSH) and malondialdehyde (MDA) using commercial kits (Bio Diagnostic, Giza, Egypt) [27].

Total antioxidant capacity was measured using a commercially available colorimetric assay kit (Bio Diagnostic, Egypt), and according to the manufacturer's instructions. The absorbance was measured at 505 nm using a spectrophotometer. TAC values were expressed as mmol Trolox equivalents per gram of tissue (mmol TE/g tissue) [28].

Briefly, GSH levels were determined by its reaction with 5,5′-dithiobis(2-nitrobenzoic acid) (DTNB), which reduces to form a yellow-coloured product. The absorbance of this compound was measured at 405 nm, and the results were expressed in mg/gT. [29], according to Ellinger et al. [30], heart and lungs MDA concentrations (nM/gT) were measured as a marker of lipid peroxidation. The concentration of reactive thiobarbituric acid species in the supernatant was measured to ascertain the MDA content. At 534 nm, the absorbance of the resulting pink product was determined.

I. Evaluation of HSP70, BDKRB1, IRF3 and STAT2 expression by quantitative RT-PCR

The Total RNA Purification Kit (Jena Bioscience, Germany, Cat. #PP-210S) was used to isolate total RNA from heart and lung tissues, and Thermo Scientific's Nanodrop ND-1000 Spectrophotometer was used to assess the RNA's concentration and purity. Using RevertAid First Strand cDNA Synthesis Kit (Thermo Scientific, USA, Cat. #K1622), reverse transcription was carried out in accordance with the manufacturer's instructions.

Using β-actin (ACTB) as the internal reference gene, a fluorescence-based real-time PCR technique was used to analyze gene expression. iQ SYBR® Green Supermix (Bio-Rad, USA, Cat. #1708880) was used to set up the reactions. For real-time RT-PCR, the primers indicated in Table 1 were utilized. Following a three-minute initial denaturation at 95°C,

there were forty cycles of denaturation (15 s at 95°C), annealing (30 s at 60°C), and extension (30 s at 72°C). Melting curve analysis was performed at the conclusion of each reaction to guarantee the specificity of the PCR products. Every experiment, including the no-template negative control (NTC), was conducted in triplicate. The 2^-ΔΔCT method was used to determine the relative gene expression levels in relation to the control [31].

TABLE 1. Primer sequence for quantitative real-time RT-PCR

Gene	Forward primer	Reverse primer	Amplicon size (bp)	Accession number
ACTB	5'-AAGTACCCCATTGAGCACGG-3'	5'-CATCTTCTCACGGTTGGCCT-3'	156	>XM_060405599.1
HSP70	5'-GATCAACGACGGAGACAAGC-3'	5'-GCTGCGAGTCGTTGAAGTAG-3'	182	>NM_001267874.1
BDKRB1	5'-CTCTTCGTGCTGTCCGTCTT-3'	5'-TGCTGATGAAGAGGTTGGCC-3'	208	>XM_027957374.3
IRF3	5'-GTCAAGGTTGTC	5'-AGAAATCCATGTCCTCGGCC-3'	172	>XM_027978627.2
STAT2	5'-GGAGTCCTAGAACCACACCC-3'	5'-TCTGGCAAGGCAATAGTGGA-3'	193	>XM_004006580.6

ACTB: Actin beta; HSP70: heat shock 70KDa protein 1A; BDKRB1: bradykinin receptor B1; IRF3: Interferon regulatory factor 3; STAT2: Signal transducer and activator of transcription 2.

J. *Environmental Data Collection*

The Egyptian Meteorological Authority (http://ema.gov.eg) provided environmental data, such as relative humidity and ambient temperature. Heat stress indicators, including the t emperature-humidity index (THI) and the estimated respiration rate (RRest), were calculated using daily meteorological records that corresponded to the sampling dates during the study period.

K. *Heat stress indices calculation*

Heat stress in sheep was assessed using the temperature-humidity index for sheep (THIsheep), which was calculated according to the established equation described by [32].

$$THI_{sheep} = AT - \{[0.31 - (0.31 \times RH/100)] \times (AT - 14.4)\}$$

where AT represents ambient temperature (°C), and RH represents relative humidity (%). Based on THIsheep values, heat stress levels were classified as no heat stress (< 22.2), moderate heat stress (22.2 to < 23.2), severe heat stress (23.2 to < 25.6), and extreme heat stress (> 25.6), following previously published thresholds [32].

Physiological heat stress was additionally evaluated using the estimated respiration rate (RRest), calculated using the equation reported by [33]:

$$RRest = 5.1\, t_{db} + 0.58\, RH - 1.7\, v_w + 0.039\, r_s - 52.8$$

Where tdb is dry-bulb temperature (°C), RH is relative humidity (%), vw is wind speed (m/s), and rs is solar radiation (W/m²). Respiration rate categories were derived using a solar radiation value of 800 W/m² and a wind speed of 0 m/s, consistent with the original model assumptions. Based on the estimated respiration rate, animals were categorized as normal (< 90 breaths/min), alert (90 - 110 breaths/min), danger (110 - 130 breaths/min), or emergency (≥ 130 breaths/min).

L. *Statistical analysis*

Data from the 19 ill-bled sheep carcasses were summarized using descriptive statistics and reported as frequencies and percentages. Simple linear regression analyses were performed to assess the relationship between each climatic variable (maximum temperature, relative humidity, and THI) and the number of cases for each condition (ill-bleeding and Bluetongue virus). The strength and direction of associations were evaluated using the Pearson correlation coefficient (r), and the proportion of variance explained was expressed as the coefficient of determination (R^2).

Associations between heat stress indicators and the occurrence of ill-bleeding or BTV were evaluated using the Fisher-Freeman-Halton exact test due to low expected cell counts (<5). Effect sizes were quantified with Cramér's V, interpreted as weak (≤0.20), moderate (>0.20-0.60), or strong (>0.60) [34].

Twelve bluetongue virus-positive ill-bled carcasses were compared to healthy control sheep for molecular and biochemical analyses to evaluate heat stress-related gene expression and oxidative stress biomarkers. Quantitative data were presented as mean ± standard deviation (SD). Data normality was assessed using the Shapiro-Wilk test. Comparisons between infected carcasses and controls were performed using a one-sample t-test, in which the mean value of the healthy control group was used as the reference (normal threshold).

Mean values obtained from bluetongue virus-positive ill-bled carcasses were further compared across months using one-way analysis of variance (ANOVA). These month-based comparisons were restricted to periods in which bluetongue-positive cases were detected and occurred under comparable levels of heat stress, as ill-bled carcasses recorded in other months were exposed to lower or variable heat stress conditions and tested negative for bluetongue virus. The magnitude of month-related effects was quantified by calculating eta squared (η^2), with effect sizes interpreted as small (0.01), moderate (0.06), or large (≥ 0.14) [35]. Effect size estimates were obtained using the effectsize package in R [36].

PASW Statistics (SPSS Inc., Chicago, IL, USA; version 18.0) was used for all statistical analyses, and $p \leq 0.05$ was the threshold for statistical significance. R software (version 4.4.3; R Foundation for Statistical Computing) was used to create graphical boxplots using the ggplot2 [37], ggpubr [38], and gridExtra [39] packages.

III. RESULTS

A. *BTV detection in ill-bled condemned sheep*

Molecular detection of Bluetongue virus (BTV) was carried out by targeting the VP7 protein gene of the viral genome. Reverse transcription polymerase chain reaction (RT-PCR) was performed on heart and lung tissue samples collected from 19 fully condemned ill-bleeding sheep carcasses. BTV was detected in 12 (10 ram and 2 ewe) of the 19 cases, representing a prevalence of 63.2% in ill bled carcasses.

B. *Pathological and immunohistochemical findings*

ISSN: 3107-6513

The internal organs of 12 cases from 19 total condemned ill-bleeding sheep carcasses exhibited pale streaks running through the myocardium (Fig. 1a). Dark brown areas appeared on subepicardial with multifocal pale anemic areas (Fig. 1a1). The microscopic findings of myocardium of sheep infected with (BTV) revealed acute diffuse epicarditis, characterized by inflammatory cells infiltration mostly macrophages, and lymphocytes, oedema and fibrin deposition (Fig. 1b). Furthermore, the myocardium displayed non-suppurative myocarditis characterized by disorganization of muscle bundles, muscle fiber fragmentation, and aggregation or diffuse infiltration of mononuclear cells among the muscle bundles (Fig. 1c and d). Perivascular oedema and leukocytic infiltration and necrosis of muscle bundles which appeared deeply eosinophilic were also noticed (Fig. 1e). A strong intensity of COX-2 expression was observed in the necrosed cardiomyocytes and inflammatory cells (Fig. 1f). Additionally, increased iNOS expression was noted in the cytoplasm of cardiomyocytes (Fig. 1g).

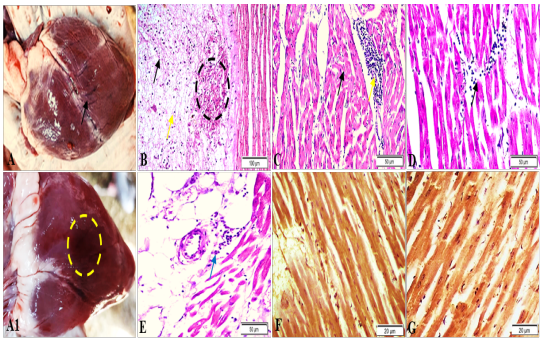

Fig. 1. Pathological examination of heart showing: Grossly, A Pale streaks running through the myocardium (black arrow). A1 Dark brown areas on subepicardial with multifocal pale anemic areas (yellow circle). B Microscopically, acute diffuse epicarditis inflammatory cells infiltration (black circle), oedema (yellow arrow) and fibrin deposition (black arrow). C Non-suppurative myocarditis, disorganization of muscle bundles (black arrow) and mononuclear cells aggregation (yellow arrow). D Muscle fiber fragmentation infiltration (black arrow). E Perivascular oedema and leukocytic infiltration and necrosis of muscle bundles (blue arrow). F Degenerated cardiomyocytes and inflammatory cells showing positive expression of Cox2. G Marked increase of iNOS expression of cardiomyocytes.

Histopathological findings of cross section of sheep infected with bluetongue virus revealed degeneration and necrosis of endothelial lining with oedema of subendothelial connective tissue accompanied with few mononuclear cell's infiltration (Fig. 2a). Tunica media demonstrated complete disorganization and severe fragmentation of elastic lamellae and accumulation of basophilic ground substance (mucopolysaccharides) and focal loss of smooth muscle cells (Fig. 2b). Tunica adventitia displayed oedema of collagenous connective tissue with disruption of fibers, few mononuclear cells infiltration and oedema of vasa vasorum wall (Fig. 2c). In the same direction, pulmonary revealed significant histopathological alterations appeared as damage and sloughing of endothelial lining in the most of examined cases. Disruption and oedema of subendothelial loss connective tissue and fragmentation of intimal collagen and elastic fibers with formation of degenerated cysts were seen in one infected case (Fig. 2d). Oedema, fragmentation and disruption of parallel elastic lamellae of tunica media were seen (Fig. 2e). Adventitial oedema with few mononuclear cell's infiltration and dilatation of vasa vasorum were noted (Fig. 2f).

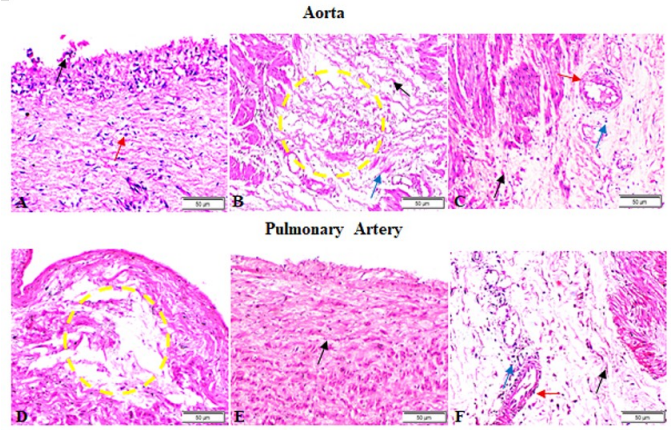

Fig. 2. Histopathological examination of aortic and pulmonary artery cross tissue sections showing: A Degeneration and necrosis of endothelial lining (black arrow) with oedema of subendothelial layer of connective (red arrow). B Complete disorganization of the tunica media (yellow circle), and severe fragmentation of elastic fibers (black arrow) and accumulation of basophilic ground substance (black arrow). C Oedema of collagenous connective tissue (black arrow), few mononuclear cells infiltration (blue arrow) and oedema of vasa vasorum wall (red arrow). D Fragmentation of intimal collagen and elastic fibers with formation of degenerated cysts (yellow circle). E Fragmentation and disruption of parallel elastic fibers (black arrow). F Adventitial oedema (black arrow) with few mononuclear cells infiltration (blue arrow) and dilatation of vasa vasorum (red arrow). (H and E,x200).

Furthermore, the liver of infected sheep by BTV displayed grossly, congestion and hepatomegaly, with dark purple-red hemorrhagic areas (Fig. 3a). Two cases yellowish hepatic parenchyma with subcapsular congested patches with marked round borders (Fig. 3a1). Microscopic examination of the hepatic tissue section revealed disorganization of hepatic cords, with marked dilatation of hepatic sinusoids and hyperplasia of Kupffer cells. Nuclear pyknosis and apoptosis of hepatocytes which appeared as deeply eosinophilic bodies scatter along hepatic lobules were noted (Fig. 3b). Fibroplasia of portal triad, mononuclear cells infiltration and hyperplasia of the bile ducts were seen (Fig. 3c). Some cases showed marked dilation of portal vein with periportal oedema and leukocytic infiltration (Fig. 3d). A fibrin thrombus was also noted in one case which attached to the tunica intima of the portal vein and accompanied by hyperplasia of bile duct which lined by high cuboidal cells (Fig. 3e). Moderate levels of COX-2 and iNOS were observed in the cytoplasm and/or nuclei of hepatocytes (Fig. 3f and g), respectively.

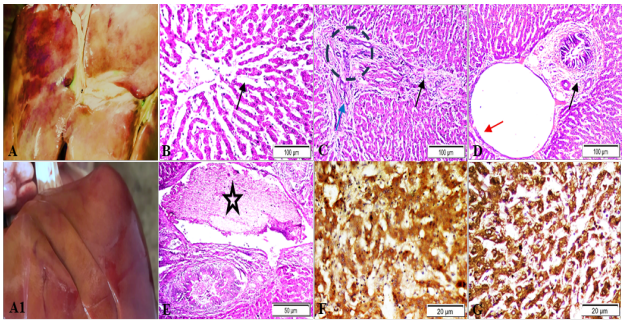

Fig. 3. Pathological examination of liver showing: Grossly, A Hepatomegaly, with dark purple-red hemorrhagic areas (yellow arrow). A1 Subcapsular

ISSN: 3107-6513

congested foci with marked round borders (black arrow). B Microscopically, disorganization of hepatic cords, with marked dilatation of hepatic sinusoids (black arrow). C Fibroplasia of portal triad (black arrow), mononuclear cells infiltration (blue arrow) and hyperplasia of the bile ducts (black circle). D Marked dilation of portal vein (red arrow) with periportal oedema and leukocytic infiltration (black arrow). E Fibrin thrombus attached to the tunica intima of the portal vein (black star). F Cytoplasmic and\or nuclear Cox2 staining of hepatocytes. G Numerous iNos stained hepatocytes.

Sheep lungs exhibited significant dark reddish to purple discoloration patches with extensive irregular pale emphysematous areas (Fig. 4a and a1). The lung tissue section revealed thickening of visceral layer of pleural membrane which appeared oedematous with few mononuclear cells infiltration in the most of examined cases (Fig. 4b). Marked ectasia of bronchioles and impaction of alveoli by eosinophilic oedematous fluid which associated with focal emphysematous areas (Fig. 4c). Extensive congestion of perialveolar capillaries and extravasation of blood cells with haemosiderin deposition (Prussian blue) were also detected (Fig. 4d and d1). Perivascular oedema and focal leukocytic aggregation composed mainly of mainly lymphocytes and macrophages (Fig. 4e). COX-2 expression was observed in the degenerated alveolar epithelium and interstitial tissue (Fig. 4f). Numerous strongly positive iNOS stained epitheliums were demonstrated in both bronchi and alveoli (Fig. 4g).

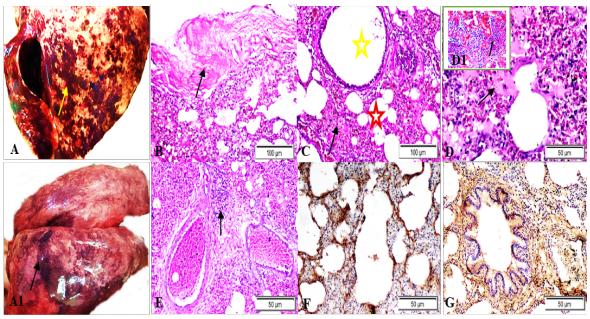

Fig. 4. Pathological examination of lung lobes showing: Grossly, A and A1 Dark reddish to purple discoloration patches (yellow arrow) with extensive irregular pale emphysematous area (black arrow), respectively. B Microscopically, thickening of visceral layer of pleural membrane (black arrow). C Dilatation of bronchioles (yellow star), intra-alveolar eosinophilic oedematous fluid (black arrow) and focal emphysematous areas (red star). D Extensive congestion of perialveolar capillaries (black arrow) and D1 extravasation of blood cells - haemoderosis deposition (Prussian blue). E Perivascular oedema (red arrow) and focal leukocytic aggregation (black arrow). F Strong Cox2 cytoplasmic staining of alveolar epithelium. G iNOS showing remarkable cytoplasmic staining of bronchial and alveolar epithelium.

Kidneys grossly revealed softening, subcapsular congestion and hemorrhages. The cross-sectional view demonstrated severe congestion of corticomedullary zone with dilatation of renal calyces and pelvis (Fig. 5a and a1). Additionally, the renal tissue sections exhibited moderate pathological alterations characterized by tubular epithelial necrosis especially in proximal convoluted tubules with intraluminal eosinophilic proteinaceous casts. Interstitial oedema and few numbers of mononuclear cells infiltration mainly lymphocytes and macrophages (Fig. 5b). Renal glomeruli displayed hypercellularity of glomerular tufts and eosinophilic proteinaceous material in Bowman's space (Fig. 5c). Some cases showed hypercellularity of glomerular tufts with damage of Bowman's capsule (Fig. 5d). On the other hand, one case showed massive damage to several glomeruli which characterized by retraction of glomerular tufts or even empty of Bowman's corpuscle from capillaries tufts (Fig. 5e). The renal tubular epithelium demonstrated strong positive cytosolic expression of COX-2 and moderate to iNOS (Fig. 5f and g), respectively.

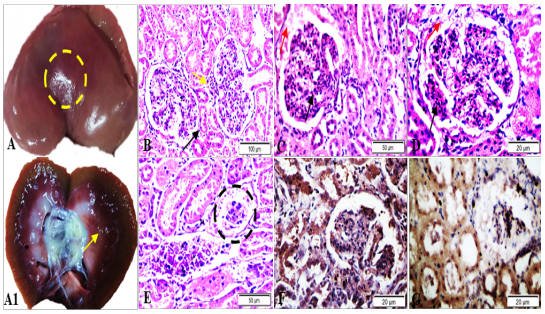

Fig. 5. Pathological examination of kidneys showing: Grossly, A subcapsular congestion and heamorrhages (black arrow). A1 Severe congestions of corticomedullary zone (yellow arrow). B Microscopically, Tubular epithelial necrosis (black arrow), interstitial oedema and few numbers of mononuclear cells infiltration (yellow arrow). C Hypercellularity of glomerular tufts (black arrow) and eosinophilic proteinaceous casts in Bowman's space (red arrow). D Hypercellularity of glomerular tufts (black arrow) and damage of Bowman's capsule (red arrow). E Retraction of glomerular tufts (black circle). F Positive expression of Cox2 in glomerular tuft and renal tubular cells. G iNOS positive expression of tubular cells.

C. Temporal distribution of ill-bleeding and BTV cases relative to heat stress indices (June 2024 - May 2025)

Fig. 6, illustrates the temporal distribution of ill-bled sheep carcasses and associated bluetongue virus (BTV) detection in relation to thermal conditions. Ill-bleeding and BTV-positive cases were predominantly observed during April–June, coinciding with progressively increasing maximum temperatures and THI values. In June 2024, all ill-bled carcasses (5/5; 100%) were BTV-positive, corresponding to extreme heat stress conditions (maximum temperature 40 °C; THI = 34.6). In contrast, February and March 2025 recorded ill-bled carcasses without BTV detection, under lower thermal load (maximum temperature 19–26.5 °C; THI 17.9–24.0).

As thermal stress intensified, BTV detection increased. In April 2025, under severe heat stress (27.5 °C; THI = 24.6), 50% (2/4) of ill-bled carcasses were BTV-positive. This trend peaked in May 2025, when extreme heat stress conditions (33.6 °C; THI = 29.6) were associated with a sharp rise in both ill-bleeding (6 cases) and BTV positivity (5/6; 83.3%).

D. Linear regression between climatic variables and ill-bleeding and bluetongue cases

Fig. 7, shows positive associations between climatic variables and sheep carcass condemnations due to ill bleeding and bluetongue. While ill-bleeding cases increased with rising temperature, humidity, and THI, these associations, despite strong correlations ($r = 0.76 - 0.81$), did not reach statistical significance ($p > 0.05$). In contrast, bluetongue cases exhibited consistently stronger and statistically significant relationships with maximum temperature ($r = 0.90$; $R^2 = 0.80$; $p = 0.039$) and THI ($r = 0.90$; $R^2 = 0.80$; $p = 0.040$), as well as a strong association with relative humidity ($r = 0.82$; $R^2 = 0.67$; $p = 0.090$). These findings highlight that bluetongue occurrence was closely linked to climatic heat-stress indicators.

ISSN: 3107-6513

E. Temporal and heat-stress-associated distribution of ill-bled sheep carcasses

Table 2 summarizes the distribution of ill-bled sheep carcasses across heat-stress categories and estimated respiration-rate classes by month and season. Most ill-bleeding cases occurred under extreme heat-stress conditions (THI > 25.6), accounting for 73.7% (14/19) of all cases, predominantly during spring and late winter. Seasonally, spring accounted for 68.4% (13/19) of ill-bled carcasses, with clear monthly clustering in May (31.6%) and June (26.3%). Both month and season showed strong and statistically significant associations with THI-based heat stress (month: Cramér's V = 0.64, p = 0.023; season: V = 0.68, p = 0.016).

Consistent patterns were observed when physiological heat stress was assessed using estimated respiration rate (RRest) (Table 2). Ill-bleeding cases were mainly recorded under moderate to extreme respiration-rate categories, with a strong and significant monthly association (V = 0.67, p = 0.006). Although seasonal differences based on RRest showed a moderate effect size (V = 0.56), this association did not reach statistical significance (p = 0.125).

F. Temporal and heat-stress-associated distribution of bluetongue virus among ill-bled sheep carcasses

Bluetongue virus (BTV) infection exhibited a marked temporal and heat-stress-related distribution among ill-bled sheep carcasses (Table 3). Seasonal analysis demonstrated that all BTV-positive carcasses occurred during spring, resulting in a statistically significant association with a strong effect size (Cramér's V = 0.68; p = 0.009). Monthly analysis revealed significant clustering in May and June, with BTV prevalences of 83.3% and 100%, respectively (Cramér's V = 0.77; p = 0.013), while no positive cases were detected in February or March.

BTV positivity was also significantly associated with extreme heat stress as defined by the Temperature–Humidity Index (THI), where 85.7% of ill-bled carcasses were BTV-positive (Cramér's V = 0.78; p = 0.002). In contrast, no BTV-positive cases were observed under severe or no heat-stress conditions. Similarly, increasing estimated respiration rate categories were associated with higher BTV prevalence, particularly under moderate to extreme physiological stress, with a moderate-to-strong effect size (Cramér's V = 0.69; p = 0.032). These findings indicate a strong association between environmental heat load, animal stress indicators, and BTV detection at slaughter (Table 3).

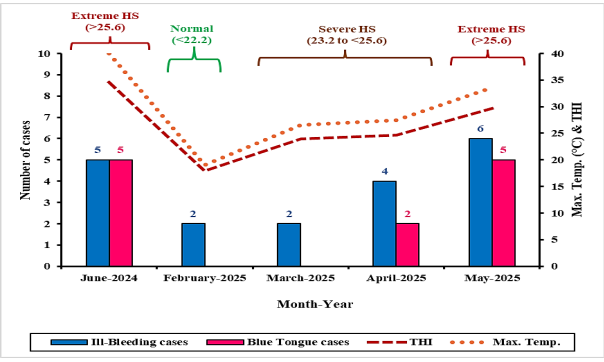

Fig. 6. Temporal distribution of ill-bleeding (N = 19) and bluetongue virus (BTV) (n = 12) cases in completely condemned sheep carcasses in relation to monthly variations in maximum ambient temperature (°C) and the temperature-humidity index for sheep (THIsheep) throughout the study period (June 2024 - May 2025). THI categories indicate levels of heat stress (HS): normal (< 22.2), severe (23.2 to < 25.6), and extreme (> 25.6). Peaks in ill-bleeding and BTV cases coincide with periods of elevated temperature and THI, while minimal case numbers are observed during months characterized by normal THI values.

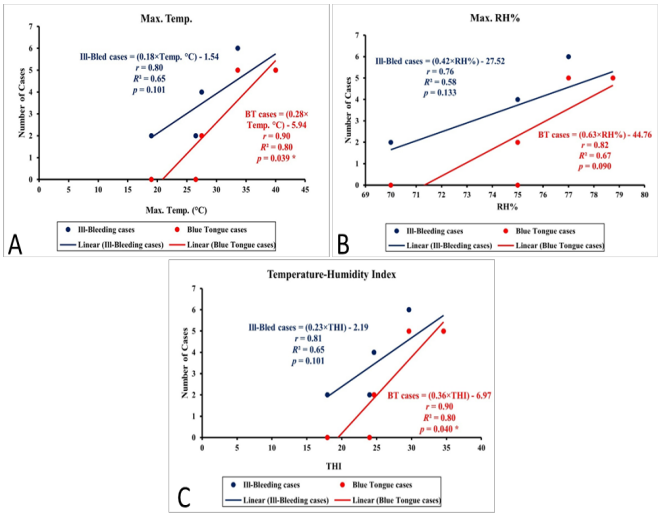

Fig. 7. Linear relationships between climatic variables and total sheep carcass condemnations attributed to ill bleeding (N = 19) and blue tongue (n = 12). Scatter plots illustrate associations between (A) maximum ambient temperature (°C), (B) maximum relative humidity (RH%), and (C) Temperature–Humidity Index (THI), with the number of condemned carcasses. Blue markers represent ill bleeding cases, and red markers represent blue tongue cases. Regression equations, Pearson correlation coefficients (r), coefficients of determination (R^2), and p values are shown for each condition. Significance was set at $p \leq 0.05$.

G. Temporal analysis of heart and lung levels of oxidative stress biomarkers in BTV-infected, ill-bled sheep

Monthly variation in oxidative stress markers in the heart and lung tissues of bluetongue virus–infected, ill-bled sheep carcasses is shown in (Fig. 8). Across all markers, values for infected animals differed markedly from healthy controls; however, no statistically significant differences were detected among April, May, and June, despite visible fluctuations in mean values. Total antioxidant capacity (TAOC) in infected animals remained markedly lower than healthy controls in both tissues (heart control = 1.07 µmol/L; lung control = 1.35 µmol/L; $p < 0.0001$).

In the heart, mean TAOC values declined slightly from 0.84±0.04 µmol/L (April) to 0.70±0.07 µmol/L (May) and 0.75±0.06 µmol/L (June), but the month effect was not significant (p = 0.081), although the effect size indicated a large magnitude ($\eta^2 = 0.43$). Similarly, TAOC in lung tissue showed minimal fluctuation (April: 0.71±0.07 µmol/L, May: 0.70±0.03 µmol/L, June: 0.75±0.05 µmol/L) with no significant month-related differences (p = 0.261; $\eta^2 = 0.26$, large effect).

Lipid peroxidation (MDA) levels in both tissues were consistently elevated compared with controls (heart control = 162.35 nmol/g; lung control = 157.39 nmol/g; $p < 0.0001$). Mean MDA concentrations in the heart increased from 171.81±0.55 nmol/g (April) to 176.28±1.66 nmol/g (May) and 178.55±6.71 nmol/g (June), but monthly differences

ISSN: **3107-6513**

TABLE 2. Distribution of ill-bleeding sheep carcasses by heat stress (THIsheep) and estimated respiration rate (RRest) across months and seasons (N= 19).

Variables	**Categories**	**THI sheep No. of ill-bleeding (%)**			**Estimated RR No. of ill-bleeding (%)**			
	Heat stress level	*Extreme*	*Severe*	*No Stress*	*Extreme*	*Severe*	*Moderate*	*Normal*
	Sheep	14 (73.7)	1 (5.3)	4 (21.1)	5 (26.3)	3 (15.8)	5 (26.3)	6 (31.6)
Month	February	0	0	2 (10.5)	0	0	0	2 (10.5)
	March	1 (5.3)	0	1 (5.3)	0	1 (5.3)	0	1 (5.3)
	April	2 (10.5)	1 (5.3)	1 (5.3)	0	0	1 (5.3)	3 (15.8)
	May	6 (31.6)	0	0	1 (5.3)	1 (5.3)	4 (21.1)	0
	June	5 (26.3)	0	0	4 (21.1)	1 (5.3)	0	0
	Cramer's V	0.64			0.67			
	P- value	0.023*			0.006*			
Season	Spring	13 (68.4)	1 (5.3)	1 (5.3)	5 (26.3)	2 (10.5)	5 (26.3)	3 (15.8)
	Winter	1 (5.3)	0	3 (15.8)	0	1 (5.3)	0	3 (15.8)
	Cramer's V	0.68			0.56			
	P- value	0.016*			0.125			

Associations were assessed using the Fisher-Freeman-Halton exact test.
Cramér's *V* was used as a measure of effect size, where values ≤ 0.20 indicate a weak association, values > 0.20 to ≤ 0.60 indicate a moderate association, and values > 0.60 indicate a strong association [34].
Bolded *p*-values & asterisk (*) denote statistically significant associations ($p \leq 0.05$).
THI [32]: Temperature-Humidity Index; heat stress (HS) categories according to THI values**:** Absence of HS (< 22.2 units); Moderate HS (22.2 to < 23.2); Severe HS (23.2 to < 25.6); and Extreme HS (> 25.6).
Estimated RR (RR_{est}): Estimated Respiration Rate; the thresholds for RR_{est} categories Brown-Brandl [33]: Normal = 90; Moderate (alert) = 90-110; Severe (danger) = 110-130; and Extreme (emergency) ≥130.

TABLE 3. Distribution and prevalence of blue tongue among ill-bled sheep carcasses by month, season, and heat stress (BT = 12/19).

Variables	**Categories**	**BT Positive**	**Total ill-bled**	**Prevalence %**	**Cramér's *V***	***p*- value**
	Cases	12	19	63.2		
Month	February	0	2	0	0.77	0.013 *
	March	0	2	0		
	April	2	4	50.0		
	May	5	6	83.3		
	June	5	5	100		
Season	Spring	12	15	80.0	0.68	0.009 *
	Winter	0	4	100		
THI	Extreme	12	14	85.7	0.78	0.002 *
	Severe	0	1	0		
	No Stress	0	4	0		
Estimated RR	Extreme	5	5	100	0.69	0.032 *
	Severe	2	3	66.7		
	Moderate	4	5	80.0		
	Normal	1	6	16.7		

Associations were assessed using the Fisher-Freeman-Halton exact test.
Cramér's *V* was used as a measure of effect size, where values ≤ 0.20 indicate a weak association, values > 0.20 to ≤ 0.60 indicate a moderate association, and values > 0.60 indicate a strong association [34].
Bolded *p*-values & asterisk (*) denote statistically significant associations ($p \leq 0.05$).
THI [32]: Temperature-Humidity Index; heat stress (HS) categories according to THI values**:** Absence of HS (< 22.2 units); Moderate HS (22.2 to < 23.2); Severe HS (23.2 to < 25.6); and Extreme HS (> 25.6).
Estimated RR (RR_{est}): Estimated Respiration Rate; the thresholds for RR_{est} categories Brown-Brandl [33]: Normal = 90; Moderate (alert) = 90-110; Severe (danger) = 110-130; and Extreme (emergency) ≥130.

ISSN: **3107-6513**

remained nonsignificant ($p = 0.267$; $\eta^2 = 0.25$, large effect). In the lung, MDA means were similarly elevated and stable across months (April: 174.18±4.99 nmol/g; May: 177.42±1.70 nmol/g; June: 175.26±2.03 nmol/g), with no significant variation ($p = 0.244$; $\eta^2 = 0.27$, large effect).

Reduced glutathione (GSH) levels in infected animals were significantly lower than those of controls (heart control = 98.65 µM/g; lung control = 91.99 µM/g; $p < 0.0001$). Heart GSH values increased modestly from 48.66±2.83 µM/g (April) to 57.14±7.04 µM/g (May) and 54.92±11.24 µM/g (June) but showed no significant monthly differences ($p = 0.545$; $\eta^2 = 0.13$, moderate effect). Lung GSH values followed a similar pattern (April: 45.33±3.77 µM/g; May: 48.40±8.90 µM/g; June: 49.46±18.60 µM/g) with no significant temporal effect ($p = 0.938$; $\eta^2 = 0.01$, small effect).

Importantly, the absence of significant month-to-month differences coincides with the fact that all three months represent a period of extreme THI and the seasonal peak of bluetongue virus activity. This period is characterized by persistent heat stress, high vector abundance, and maximal infection pressure, resulting in a consistently high level of oxidative stress across months. Thus, although moderate-to-large effect sizes were detected for some markers, the uniform and sustained environmental and infectious stress load likely minimized temporal variability, producing statistically comparable oxidative profiles throughout the peak THI/BTV period.

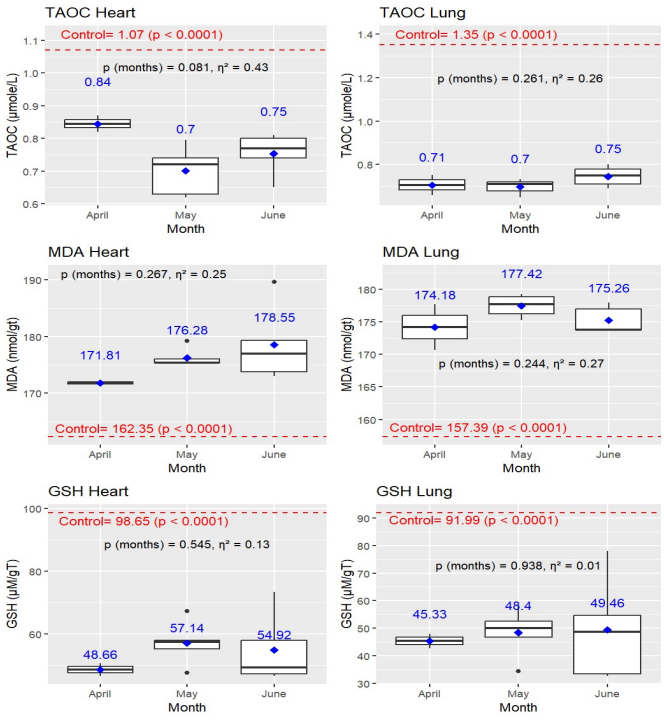

Fig. 8. Monthly variation in oxidative stress markers in the heart and lung of bluetongue virus-infected, ill-bled sheep carcasses (n = 12). Boxplots illustrate the distribution of oxidative stress marker levels across months, with mean values indicated by blue symbols and annotated numerically. Oxidative stress marker levels of healthy control animals were plotted as a horizontal reference line (control), and comparisons between infected and control groups were performed using a one-sample t-test ($p \leq 0.05$). Statistical comparisons among months were conducted using one-way ANOVA ($p \leq 0.05$). Effect sizes were estimated using eta squared (η^2) to quantify the magnitude of month-related differences and were interpreted as small (~0.01), moderate (~0.06), or large (≥ 0.14).

H. Temporal analysis of heart and lung expression of stress- and immune-related genes in BTV-infected, ill-bled sheep

Fig. 9, illustrates the monthly variation in heart expression levels of BDKRB1, HSP70, IRF3, and STAT2 in bluetongue virus-infected, ill-bled sheep carcasses. For BDKRB1, mean expression levels increased from 1.40±0.55 in April to 1.75±0.43 in May and 1.85±0.11 in June, all of which were significantly higher than the healthy control reference (control = 1; one-sample t-test, $p < 0.0001$). However, no statistically significant effect of month was detected ($p = 0.340$), despite a moderate effect size ($\eta^2 = 0.21$). Similarly, HSP70 expression remained elevated relative to controls across all months (means: 2.31±0.91 in April, 2.70±0.56 in May, and 1.95±0.40 in June; $p < 0.0001$ vs. control), with no significant month-to-month differences ($p = 0.151$), although a moderate effect size was observed ($\eta^2 = 0.34$).

In contrast, IRF3 expression remained consistently downregulated relative to controls, with mean values of 0.60±0.26 in April, 0.55±0.27 in May, and 0.52±0.17 in June ($p < 0.0001$ vs. control), showing no significant monthly variation ($p = 0.915$) and a negligible effect size ($\eta^2 = 0.02$). For STAT2, mean expression values were 1.64±0.37 in April, 1.85±0.18 in May, and 1.41±0.28 in June, all significantly higher than the control level ($p < 0.0001$). Although the effect of month did not reach statistical significance ($p = 0.067$), a large effect size was observed ($\eta^2 = 0.45$), indicating a trend toward month-dependent variation.

Fig. 10, depicts the monthly variation in lung expression levels of BDKRB1, HSP70, IRF3, and STAT2 in bluetongue virus-infected, ill-bled sheep carcasses. Pulmonary BDKRB1 expression was markedly elevated relative to the healthy control reference (control = 1), with mean values of 8.06±1.37 in April, 7.91±1.94 in May, and 7.08±1.81 in June (one-sample t-test, $p < 0.0001$). However, no statistically significant effect of month was observed ($p = 0.724$), and the effect size was small ($\eta^2 = 0.07$), indicating limited temporal variation.

For HSP70, mean pulmonary expression values were 0.42±0.13 in April, 0.83±0.11 in May, and 0.53±0.32 in June, remaining significantly lower than the control level ($p = 0.001$). Although monthly differences did not reach statistical significance ($p = 0.089$), a large effect size was observed ($\eta^2 = 0.42$), suggesting a trend toward month-dependent variation in pulmonary HSP70 expression.

Pulmonary IRF3 expression was consistently downregulated relative to controls across all months, with mean values of 0.10±0.04 in April, 0.17±0.06 in May, and 0.19±0.09 in June ($p < 0.0001$ vs. control). No significant effect of month was detected ($p = 0.344$), despite a moderate effect size ($\eta^2 = 0.21$), indicating relatively stable suppression of IRF3 expression over time. Similarly, STAT2 expression in lung tissue remained significantly lower than control levels (means: 0.17±0.03 in April, 0.28±0.15 in May, and 0.34±0.27 in June; $p < 0.0001$), with no significant monthly variation ($p = 0.638$) and a small effect size ($\eta^2 = 0.10$). This pattern contrasts with the cardiac tissue response, underscoring tissue-specific regulation of stress- and immune-related genes in ill-bled sheep carcasses.

ISSN: **3107-6513**

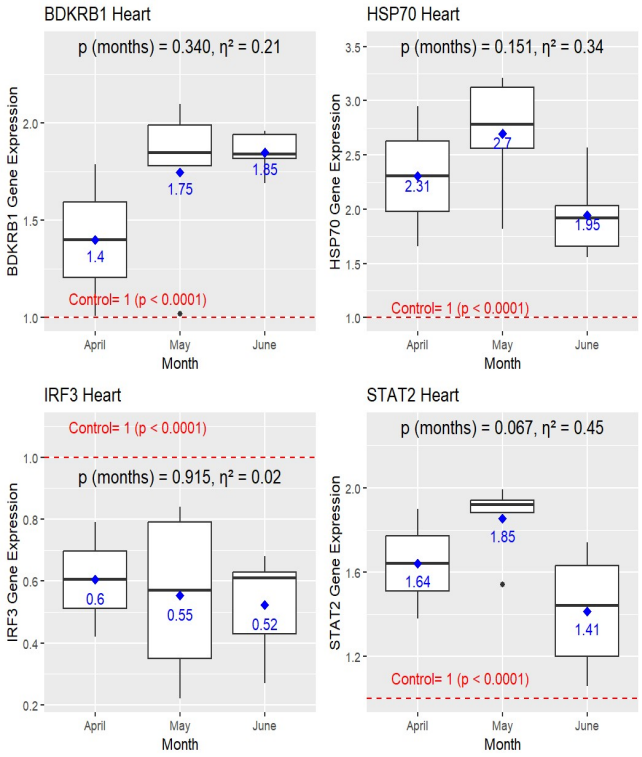

Fig. 9. Monthly variation in heart gene expression levels in bluetongue virus-infected, ill-bled sheep carcasses (n = 12). Boxplots illustrate the distribution of gene expression across months, with mean values indicated by blue symbols and annotated numerically. Gene expression levels of healthy control animals were plotted as a horizontal reference line (control = 1), and comparisons between infected and control groups were performed using a one-sample *t*-test ($p \leq 0.05$). Statistical comparisons among months were conducted using one-way ANOVA ($p \leq 0.05$). Effect sizes were estimated using eta squared (η^2) to quantify the magnitude of month-related differences and were interpreted as small (~0.01), moderate (~0.06), or large (≥ 0.14).

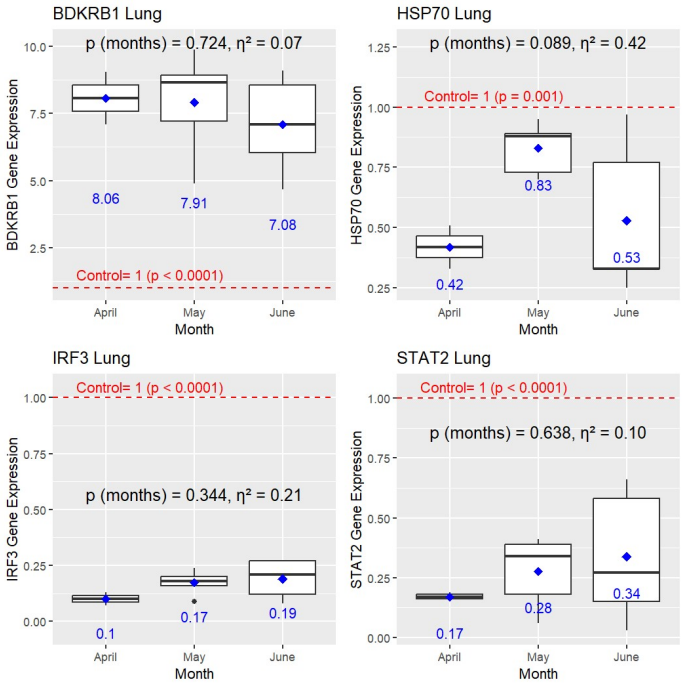

Fig. 10 Monthly variation in lung gene expression levels in bluetongue virus-infected, ill-bled sheep carcasses (n = 12). Boxplots illustrate the distribution of gene expression across months, with mean values indicated by blue symbols and annotated numerically. Gene expression levels of healthy control animals were plotted as a horizontal reference line (control = 1), and comparisons between infected and control groups were performed using a one-sample t-test ($p \leq 0.05$). Statistical comparisons among months were conducted using one-way ANOVA ($p \leq 0.05$). Effect sizes were estimated using eta squared (η^2) to quantify the magnitude of month-related differences and were interpreted as small (~0.01), moderate (~0.06), or large (≥ 0.14).

IV. Discussion

The relationship between climate change and its emergence as a major factor influencing the dynamics of infectious diseases, particularly vector-borne viral diseases like Bluetongue Virus (BTV) affecting sheep, is thoroughly examined in this descriptive case. Ill bleeding has been identified as a clinical indicator of underlying vascular injury. BTV is an arbovirus that is dependent on climate conditions and is primarily transmitted through Culicoides vectors, posing a considerable threat to both domestic and wild ruminant populations, especially sheep [9]. The disease presents various clinical manifestations, including pyrexia, oedema, mucosal lesions, and bleeding disorders, which result from damage to the endothelial cells that line blood vessels [40].

Ill bleeding was frequently observed as a reason for carcass condemnation in the cases studied, with macroscopic lung lesions characterized by pronounced dark reddish to purple discoloration and widespread irregular patches of congestion and haemorrhage. These results are consistent with descriptions provided by Paessler and Walker [41], indicating that BTV may disrupt normal haemostatic processes by impairing platelet function and coagulation pathways. The hypoxia that arises from vascular obstruction and thrombosis further intensifies tissue damage and the propensity for bleeding. Collectively, these mechanisms explain the ill bleeding observed in severe bluetongue disease, particularly in highly susceptible species such as sheep. Previous research by O'Neill [42] demonstrated that when animals are subjected to stressors, such as those induced by extreme climatic conditions, their bodies initiate the fight-or-flight response, a physiological mechanism that prepares the organism for immediate action. This response is predominantly regulated by the sympathetic nervous system, which stimulates the release of adrenaline (epinephrine) and noradrenaline (norepinephrine). Therefore, intense vasoconstriction limits peripheral blood drainage and promotes retention of blood within muscle tissues and internal organs. This physiological response contributes directly to incomplete bleeding and the dark, congested appearance observed in ill-bled carcasses.

Histopathological assessments revealed disorganization and paleness of myocardium muscle bundles, which are accompanied with non-suppurative myocarditis. This includes cardiomyocytes necrosis, fragmentation of muscle fibers and infiltration of inflammatory cells, primarily macrophages and lymphocytes. This is consistent with findings by Singh et al. [43], which showed that BTV-infected sheep heart displayed necrosis, perivascular cuffing with lymphocytes, inflammatory cell infiltration among the cardiac muscle fibers, and degeneration of those fibers. Furthermore, studies by Saminathan et al. [44] demonstrated the presence of haemorrhages and congestion in the myocardium and epicardium, and mononuclear cell infiltration in the myocardium.

Further systemic involvement was observed. The lung tissue exhibited pneumonia, characterized by vasculitis of the interstitial pulmonary blood vessels, damage to the vascular walls, and extravasation of red blood cells and eosinophilic oedematous fluid in the alveolar spaces. In a similar direction, Cecco et al. [45] reported that the alterations in the lungs, which included congestion, significant interlobular oedema, and sloughed endothelial cells along with inflammatory cells in the lumen of the pulmonary arterioles. Necrosis and the loss of the muscular layer were noted in the pulmonary artery, accompanied by hemorrhages in the interstitial tissue. These alterations align with the findings of Saminathan et al. [44], who reported significant oedema with eosinophilic exudates, swollen endothelial cells, severe congestion of inter-alveolar capillaries, and hemorrhages in the alveolar lumen and surrounding blood vessels.

An examination of the aortic wall revealed degeneration and sloughing of endothelial lining, widened interstitial spaces within the tunica media, fragmentation of elastic fibers, separation of smooth muscle fibers, and mild inflammation. These results align with those of Singh et al. [43], who reported BTV-associated endothelial injury with mild muscle fiber degeneration in the tunica medial layer of the aorta. Both the subintimal and tunica medial layers of the aorta showed fragmentation and necrosis.

The pulmonary artery showed desquamation of the endothelial lining of the tunica intima, moderate vasculitis, widening of the tunica adventitia and mild inflammation-paralleling findings by Singh et al. [43], where tunica intima of pulmonary artery showed necrosis with nuclear debris observed in sheep affected by BTV.

In the liver, a thrombus was noted to be attached to the tunica intima of the portal vein accompanied with mononuclear infiltration of portal triad. However, according to Singh et al. [43], reported the liver showed swollen endothelial cells, perivascular edema, necrosis, sinusoidal congestion and hemorrhages, and infiltration of inflammatory cells.

Additionally, microscopic renal examinations conducted in this study revealed moderate pathological changes characterized by hyperplasia of the glomerular tuft, necrosis of the tubular epithelium, and moderate inflammatory cells infiltration. Similarly, Padmini et al. [46] indicated that the kidneys of infected sheep displayed hypercellularity of mesangial cells, degeneration of renal tubules, and multifocal infiltration of lymphocytes.

Immunohistochemical analysis demonstrated an increased expression of COX-2 and iNOS in tissues affected by BTV. These molecules serve as crucial mediators of inflammation and oxidative stress. Previous studies have suggested COX-2 upregulation during the pathogenesis of BTV infection in sheep. They assessed the responses of primary sheep lung microvascular endothelial cells to BTV infection, which resulted in elevated levels of cytokines and inflammatory mediators such as IL-1, IL-6, IL-8, COX-2, and iNOS [47]. Furthermore, BTV-infected peripheral blood mononuclear cells (PBMC) from various ruminant species, specifically sheep and goats, release inflammatory cytokines [48], resulting in the overexpression of IL-1, IL-6, IL-8, IL-10, IFN-γ, TNF, and iNOS [49].

Climate change is linked to rising ambient temperatures and an increase in the frequency of heat waves, which subject ruminants to heat stress [50]. Heat stress disrupts cellular homeostasis and activates several stress-response pathways, leading to heightened expression of COX-2 and iNOS, two essential markers involved in inflammation and oxidative stress [20].

Elevated temperatures lead to an increase in mitochondrial activity while simultaneously impairing electron transport chains, which results in the excessive generation of reactive oxygen species (ROS) [51]. These ROS function as signaling molecules that activate redox-sensitive transcription factors, such as NF-κB and AP-1, which in turn directly enhance the transcription of COX-2 and iNOS genes [52]. Pro-inflammatory cytokines such as TNF-α, IL-1β, and IL-6 are released in response to heat stress [53]. These cytokines initiate intracellular signaling cascades, notably the MAPK and NF-κB pathways, which lead to an increased expression of COX-2 and iNOS. COX-2 facilitates the synthesis of prostaglandins, whereas iNOS elevates nitric oxide (NO) production, thereby intensifying the inflammatory response [54].

Furthermore, heat stress can induce vascular dysfunction and tissue hypoxia due to changes in blood flow and dehydration [55]. Under hypoxic conditions, hypoxia-inducible factor-1α (HIF-1α) is activated, which has been demonstrated to stimulate iNOS expression and collaborate with inflammatory pathways to boost COX-2 levels [56]. Therefore, heat stress increases disease susceptibility and aggravates lesions, especially vascular ones, in accordance with the observations of the current study.

By upsetting the relationships between the host, the pathogen, and the environment, all crucial elements of disease and climate change dramatically alter the epidemiology of vector-borne viral diseases in sheep [57]. The increases in temperature, and the occurrence of more frequent extreme events associated with climate change enhance the fitness and feeding behavior of vectors. Given that vector-host contact rates are heavily influenced by climate, these changes contribute to a heightened transmission of viral diseases, including BTV [58]. The environmental disturbances driven by climate change present substantial public health challenges (SDG 3) and threaten the sustainability of livestock, particularly in resource-constrained environments. An increasing body of evidence suggests that climate change has a significant impact on livestock health, as cardiopulmonary dysfunction resulting from heat stress or BTV infection illustrates the synergistic effects of environmental stressors and infectious diseases [59].

Our research revealed that BTV was identified in 12 out of 19 instances. Most positive cases were noted during the warmer seasons, especially in spring and early summer. Climatic interactions manifest through the spatial and temporal distribution of Culicoides vectors [60]. In South Africa and Kenya, the seasonal prevalence of adult C. imicola is closely associated with rainfall from previous months, while predictive models in Iberia, Morocco, and South Africa underscore the significance of mean annual temperatures during both the coldest and warmest periods [61]. Prevalence of bluetongue in sheep varies widely by region, ranging from 12.9% to 65% in different studies and locations [62,63,64]. Our investigation has documented elevated MDA levels alongside diminished TAC

and GSH concentrations in cardiac and pulmonary tissues under extreme temperature–humidity index conditions. Heat stress (HS), which raises free radical production above the body's antioxidant capacity and causes oxidative damage and disruption of antioxidant defense mechanisms, is attributed for these alterations [65,66,67]. Consistent with this, Rebez et al. [68] illustrated that climate-related stress in sheep disturbs the oxidant–antioxidant equilibrium, as indicated by heightened blood MDA and cortisol levels, along with significant decreases in TAC and GSH. Similarly, Bouzar et al. [69] demonstrated that BTV infection boosts the generation of reactive oxygen species (ROS) in endothelial cells due to the localization of BTV-associated proteins within mitochondria, a process linked to increased expression of cytokines and inflammatory mediators. In the current study, the expression levels of BDKRB1 and HSP70 were significantly elevated in cardiac tissues, while BDKRB1 expression was also heightened in lung samples during spring and early summer. These stress-responsive proteins are crucial for cellular adaptation to various stressors, including heat, cold, oxidative stress, and infection, by safeguarding cells from damage and facilitating survival and recovery processes [70,71]. Rouhiainen et al. [72] noted that thermal stress significantly modifies BDKR expression, a vital mediator of inflammatory responses. The observed increase in BDKRB1 expression indicates that heat stress (HS) initiates inflammation and tissue damage, which in turn promotes the release of pro-inflammatory cytokines, increases vascular permeability, and leads to the infiltration of immune cells. This investigation also noted an increase in HSP70 mRNA levels in response to heat stress (HS), aligning with earlier research conducted on sheep [72]. Borges et al. [73] indicated that HSP70, recognized as one of the most thoroughly examined heat shock proteins in sheep, is stimulated by HS and functions as a molecular chaperone. It promotes the breakdown of damaged proteins, prevents protein aggregation, and helps proteins fold and refold correctly. Additionally, HSP70 affects inflammatory responses by interacting with different interleukins and cytokines like TNF-α. Conversely, we observed a reduction in HSP70 levels in the lungs. In contrast, other studies, such as those by Singh et al. [43], found that HSP70 levels in the spring were lower compared to other seasons, as the climatic conditions during spring were more conducive for sheep. The average Temperature-Humidity Index (THI) values during the noon hours in summer (31.54) and fall (23.60) exceeded those recorded in winter and spring. Some research indicates that cells from sheep breeds that are better adapted to heat produce lower concentrations of HSP70 compared to those from less adapted breeds [74]. Likewise, in sheep acclimatized to desert conditions, HSP70 levels were found to be higher than in their less adapted counterparts [75]. The infection caused by the Bluetongue virus (BTV) has been demonstrated to trigger cellular stress responses, which include the upregulation of heat shock proteins like HSP70 [76,77]. During BTV infection, the process of viral replication and the resultant oxidative stress disrupt normal cellular functions, leading to the activation of HSP70 expression as a protective mechanism [78]. In addition to being essential for maintaining protein integrity, elevated HSP70 influences the host's immune response by interacting with pro-inflammatory cytokines like TNF-α and interleukins, which may impact the degree of inflammation brought on by BTV [79]. Furthermore, some research indicates that HSP70 might directly engage with viral proteins, facilitating either viral assembly or replication, thereby underscoring its dual function in cellular protection and viral dissemination [80]. Consequently, HSP70 serves as a significant mediator in the interaction between host and pathogen during BTV infection, connecting cellular stress responses to inflammatory pathways and the pathogenesis of the virus [81]. Our research revealed a downregulation of IRF3 in samples taken from the heart and lungs. Conversely, we observed an increased expression of STAT2 in heart samples, while lung tissues exhibited a downregulation. BTV has developed various mechanisms to circumvent the host's antiviral immune response, particularly targeting the type I interferon (IFN) pathway. Two essential elements of this pathway are IRF3 and STAT2 [82]. IRF3 functions as a transcription factor that, upon viral infection, undergoes phosphorylation and is translocated into the nucleus to initiate the expression of type I interferons (IFN-α/β). The infection by BTV can activate IRF3 early in the infection process, thereby initiating an antiviral response [83]. However, specific BTV proteins, such as NS3, have the capability to inhibit the phosphorylation or nuclear translocation of IRF3, consequently suppressing the production of IFN and attenuating the host's antiviral response [82]. STAT2 is an integral component of the JAK-STAT signaling pathway, which mediates the cellular response to type I interferons [83]. Following the binding of IFN to its receptor, STAT2 forms a complex with STAT1 and IRF9, which is then translocated into the nucleus to enhance the transcription of interferon-stimulated genes (ISGs) that serve to inhibit viral replication [84]. BTV has been demonstrated to disrupt STAT2 signaling, either by enhancing its degradation or by inhibiting its phosphorylation, which consequently hinders ISG induction and promotes viral replication [85]. Certain studies indicate that BTV infection may result in the proteasomal degradation of IRF3 or the inhibition of it signaling pathway in infected cells, especially within cardiac and pulmonary tissues, where viral replication is prevalent [83,86] Conversely, the heart may exhibit reduced viral replication or a delayed suppression mediated by viral proteins, thereby enabling host cells to upregulate STAT2 as a compensatory antiviral mechanism [87]. An increase in STAT2 levels in the heart could signify the activation of interferon signaling aimed at controlling viral dissemination within this organ, which is vital for survival [88]. This tissue-specific variation may also be affected by differences in the local cytokine environment, immune cell infiltration, or stress responses, which can variably influence STAT2 expression [89]. BTV produces proteins such as NS3 and NS4, which can facilitate the degradation of STAT2 or inhibit its phosphorylation, thereby diminishing its activity [88]. The lung serves as a primary site for BTV replication, and the viral load may be elevated in this region, resulting in a more pronounced suppression of STAT2, which leads to lower levels of STAT2. This decline reduces ISG expression and compromises the local antiviral response, thereby promoting viral replication in lung tissues [89].

In interpreting this study's findings, several limitations should be acknowledged: Sample Size and Statistical Power: Although biologically relevant trends were found in oxidative stress markers (MDA, TAC and GSH), the relatively small number of samples (n = 19) make interpretation difficult. Variables in the environment and breeds could introduce heterogeneity and mask more consistent responses (e.g.,

microclimate fluctuations, breed-specific thermotolerance levels).

V. Conclusion

Climate change is closely associated with livestock health, showing that heat stress, indicated by higher temperature-humidity indices, contributes to the emergence and severity of Bluetongue virus (BTV) in sheep. BTV was identified in ill-bleeding carcasses, supported by molecular analysis, pathological findings, and biochemical evaluations of oxidative stress.

Acknowledgment

We sincerely acknowledge for all members in the Al-Basatin automated slaughterhouse and 15 May Semi-Automated Abattoir for the support and valuable assistance they provided during the research process.

References

[1] Owusu-Sekyere E, Nyam YS, Selelo OT, Torsu DA (2024) Sustainable Development Goal 13: Urgent action to combat climate change and its impacts. In: Handbook on public policy and food security. Edward Elgar Publishing, Cheltenham.

[2] Kassem A, Khattab MS, Ismael E, Osman AH (2025) Impact of climate change on ruminant health and Emerging Diseases in Egypt. J Appl Vet Sci 10:106–117.

[3] Kassem A, Khattab MS, Ismael E, Yassin AM, Hamza D,Osman AH (2025) Climate change and the emergence of Rift Valley fever virus: a pathological and environmental study of sheep jaundice in Egyptian slaughterhouses. BMC Vet Res 21:539.

[4] Marcone G (2024) Comparative welfare evaluation of sheep production systems. [Book Section/Report] pp 73–75.

[5] Sithole SM, Nephawe KA, Mphaphathi ML, Ngcobo JN (2025) Understanding the role of long-chain polyunsaturated fatty acid and antioxidants in enhancing rooster semen quality: a comprehensive review. Front Anim Sci 6:1669519.

[6] Boni R (2019) Heat stress, a serious threat to reproductive function in animals and humans. Mol Reprod Dev 86:1307–1323.

[7] Haque MN, Rahman MH, Naher L, Udoy SAK, Ali MZ, Ahmed S (2025) Comprehensive review of emerging insights into bluetongue virus in small ruminants with emphasis on epidemiology, diagnosis and control in Bangladesh and South Asia. Discov Anim 2:76.

[8] Kampen H, Werner D (2023) Biting midges (Diptera: Ceratopogonidae) as vectors of viruses. Microorganisms 11:2706.

[9] Brand SP, Keeling MJ (2017) The impact of temperature changes on vector-borne disease transmission: Culicoides midges and bluetongue virus. J R Soc Interface 14:20160481.

[10] De Souza WM, Weaver SC (2024) Effects of climate change and human activities on vector-borne diseases. Nat Rev Microbiol 22:476–491.

[11] Ozmen O, Kale M, Haligur M, Yavru S, Yavru S (2009) Pathological, serological, and virological findings in sheep infected simultaneously with Bluetongue, Peste-des-petits-ruminants, and Sheeppox viruses. Trop Anim Health Prod 41:951–958.

[12] Caporale M, Di Gialleonorado L, Janowicz A, Wilkie G, Shaw A, Savini G, Palmarini M (2014) Virus and host factors affecting the clinical outcome of bluetongue virus infection. J Virol 88:10399–10411.

[13] Chauhan SS, Rashamol VP, Bagath M, Sejian V, Dunshea FR (2021) Impacts of heat stress on immune responses and oxidative stress in farm animals and nutritional strategies for amelioration. Int J Biometeorol 65:1231–1244.

[14] Howerth EW (2015) Cytokine release and endothelial dysfunction: a perfect storm in orbivirus pathogenesis. Vet Ital 51:275–281.

[15] Mohammed A, Abdulai A, Birteeb PT, Husssein SMA (2018) Major causes of organ and carcass condemnations of cattle and their associated financial loss at the Tamale abattoir, Ghana. UDS Int J Dev 5:53–67.

[16] Bhattarai A, Shah S, Bagherieh S, Mirmosayyeb O, Thapa S, Paudel S, Khanal P (2022) Endothelium, platelets, and coagulation factors as the three vital components for diagnosing bleeding disorders: a simplified perspective with clinical relevance. Int J Clin Pract 2022:5369001.

[17] Mehrbod P, Ande SR, Alizadeh J, Rahimizadeh S, Shariati A, Malek H, Ghavami S (2019) The roles of apoptosis, autophagy and unfolded protein response in arbovirus, influenza virus, and HIV infections. Virulence 10:376–413.

[18] Guillin OM, Vindry C, Ohlmann T, Chavatte L (2019) Selenium, selenoproteins and viral infection. Nutrients 11:2101.

[19] Sánchez-Cordón PJ, Pedrera M, Risalde MA, Molina V, Rodríguez-Sánchez B, Nunez A, Gómez-Villamandos JC (2013) Potential role of proinflammatory cytokines in the pathogenetic mechanisms of vascular lesions in goats naturally infected with bluetongue virus serotype 1. Transbound Emerg Dis 60:252–262.

[20] Aryal B, Kwakye J, Ariyo OW, Ghareeb AF, Milfort MC, Fuller AL, Aggrey SE (2025) Major Oxidative and Antioxidant Mechanisms During Heat Stress-Induced Oxidative Stress in Chickens. Antioxidants 14:471.

[21] Lwanga SK, Lemeshow S (1991) Sample size determination in health studies. World Health Organization, Geneva.

[22] Regassa A, Moje N, Megersa B, Beyene D, Sheferaw D, Debela E, Skjerve E (2013) Major causes of organs and carcass condemnation in small ruminants slaughtered at Luna Export Abattoir, Oromia Regional State, Ethiopia. Prev Vet Med 110:139–148.

[23] Chaurand P, Latham JC, Lane KB, Mobley JA, Polosukhin VV, Wirth PS, Caprioli RM (2008) Imaging mass spectrometry of intact proteins from alcohol-preserved tissue specimens: bypassing formalin fixation. J Proteome Res 7:3543–3555.

[24] Adedayo AD, Tijani AA, Musa AA, Adeniyi TD (2011) Histological study of smoke extract of Tobacco nicotiana on the heart, liver, lungs, kidney, and testes of male Sprague-Dawley rats. Niger Med J 52:217–222.

[25] Hall AP, Davies W, Stamp K, Clamp I, Bigley A (2013) Comparison of computerized image analysis with traditional semiquantitative scoring of Perls' Prussian Blue stained hepatic iron deposition. Toxicol Pathol 41:992–1000.

[26] Berg J, Fellier H, Christoph T, Grarup J, Stimmeder D (1999) The analgesic NSAID lornoxicam inhibits cyclooxygenase (COX)-1/-2, inducible nitric oxide synthase (iNOS), and the formation of interleukin (IL)-6 in vitro. Inflamm Res 48:369–379.

[27] Suresh DR, Annam V, Pratibha K, Prasad BM (2009) Total antioxidant capacity–a novel early bio-chemical marker of oxidative stress in HIV infected individuals. J Biomed Sci 16:61.

[28] Tabart J, Kevers C, Pincemail J, Prasad BM (2010) Evaluation of spectrophotometric methods for antioxidant compound measurement in relation to total antioxidant capacity in beverages. Food Chem 120:607–614.

[29] Kehili HE, Zerizer S (2024) Immune-stimulating and antioxidant properties of a traditional Algerian plant combination: Date fruit (Phoenix dactylifera) and Fenugreek seeds (Trigonella foenum-graecum). N Afr J Food Nutr Res 8:253–261.

[30] Ellinger S, Müller N, Stehle P, Ulrich-Merzenich G (2011) Consumption of green tea or green tea products: is there an evidence for antioxidant effects from controlled interventional studies? Phytomedicine 18:903–915.

[31] Yilmaz A, Onen HI, Alp E, Menevse S (2012) Real-time PCR for gene expression analysis. IntechOpen 12:229–254.

[32] Auguie B, Antonov A (2017) gridExtra: miscellaneous functions for "grid" graphics. R package version 2(1).

[33] Brown-Brandl TM (2018) Understanding heat stress in beef cattle. Rev Bras Zootec 47:e20160414.

[34] Cramér H (1999) Mathematical methods of statistics. Princeton University Press 43.

[35] Lakens D (2013) Calculating and reporting effect sizes to facilitate cumulative science: a practical primer for t-tests and ANOVAs. Front Psychol 4:863.

[36] Ben-Shachar MS, Lüdecke D, Makowski D (2020) Effect Size: Estimation of Effect Size Indices and Standardized Parameters. J Open Source Softw 5:2815.

[37] Wickham H, Chang W, Henry L, Pedersen TL, Takahashi K, Wilke C, van Den Brand T (2007) ggplot2: Create Elegant Data Visualisations Using the Grammar of Graphics. R package.

[38] Kassambara A (2018) ggpubr: 'ggplot2' based publication ready plots. R package version 2.

[39] Auguie B (2010) gridExtra: Miscellaneous Functions for "Grid" Graphics. R package version 2(1):292.

[40] Ozmen O, Kale M, Haligur M, Yavru S (2009) Pathological, serological, and virological findings in sheep infected simultaneously with Bluetongue, Peste-des-petits-ruminants, and Sheeppox viruses. Trop Anim Health Prod 41:951–958.

[41] Paessler S, Walker DH (2013) Pathogenesis of the viral hemorrhagic fevers. Annu Rev Pathol 8:411–440.

[42] O'Neill HA (2019) A review on the involvement of catecholamines in animal behaviour. S Afr J Anim Sci 49:1–8.

[43] Singh R, Singh KP, Singh R, Singh V, Sharma G, Kumar B, Prasath NB (2022) Renal pathological changes in sheep infected with BTV-1 during early pregnancy. Indian J Vet Pathol 46:271–276.

[44] Saminathan M, Singh KP, Maity M, Vineetha S, Manjunathareddy GB, Dhama K, Gupta VK (2021) Pathological and immunological characterization of bluetongue virus serotype 1 infection in type I interferons blocked immunocompetent adult mice. J Adv Res 31:137–153.

[45] Cecco BSD, Santos IRD, Molossi FA, Canal CW, Barros CSLD, Driemeier D, Pavarini SP (2023) Viral diseases of sheep in Brazil: a review and current status. Ciênc Rural 53:e20220218.

[46] Padmini V, Hemanth I, Devi RV, Rao ST, Chowdary CSR (2024) Pathomorphology of spontaneous kidney lesions in slaughtered pigs. Indian J Vet Pathol 48:12–17.

[47] DeMaula CD, Leutenegger CM, Bonneau KR, MacLachlan NJ (2002) The role of endothelial cell-derived inflammatory and vasoactive mediators in the pathogenesis of bluetongue. Virology 296:330–337.

[48] Singh A, Prasad M, Mishra B, Manjunath S, Sahu AR, Priya GB, Gandham RK (2017) Transcriptome analysis reveals common differential and global gene expression profiles in bluetongue virus serotype 16 (BTV-16) infected peripheral blood mononuclear cells (PBMCs) in sheep and goats. Genom Data 11:62–72.

[49] Channappanavar R, Singh KP, Singh R, Umeshappa CS, Ingale SL, Pandey AB (2012) Enhanced proinflammatory cytokine activity during experimental bluetongue virus-1 infection in Indian native sheep. Vet Immunol Immunopathol 145:485–492.

[50] Joy A, Dunshea FR, Leury BJ, Clarke IJ, DiGiacomo K, Chauhan SS (2020) Resilience of small ruminants to climate change and increased environmental temperature: A review. Animals 10:867.

[51] Belhadj Slimen I, Najar T, Ghram A, Dabbebi H, Ben Mrad M, Abdrabbah M (2014) Reactive oxygen species, heat stress and oxidative-induced mitochondrial damage. A review. Int J Hyperthermia 30:513–523.

[52] Le Rossignol S, Ketheesan N, Haleagrahara N (2018) Redox-sensitive transcription factors play a significant role in the development of rheumatoid arthritis. Int Rev Immunol 37:129–143.

[53] Liu YL, Ding KN, Shen XL, Liu HX, Zhang YA, Liu YQ, Tang LP (2022) Chronic heat stress promotes liver inflammation in broilers via enhancing NF-κB and NLRP3 signaling pathway. BMC Vet Res 18:289.

[54] Pérez-Sala D, Lamas S (2001) Regulation of cyclooxygenase-2 expression by nitric oxide in cells. Antioxid Redox Signal 3:231–248.

[55] Sejian V, Hyder I, Maurya VP, Bagath M, Krishnan G, Aleena J, Naqvi SMK (2017) Adaptive mechanisms of sheep to climate change. In: Sheep production adapting to climate change. Springer Singapore, Singapore, pp 117–147.

[56] Korbecki J, Simińska D, Gąssowska-Dobrowolska M, Listos J, Gutowska I, Chlubek D, Baranowska-Bosiacka I (2021) Chronic and cycling hypoxia: drivers of cancer chronic inflammation through HIF-1 and NF-κB activation: a review of the molecular mechanisms. Int J Mol Sci 22:10701.

[57] Wilcox BA, Echaubard P, de Garine-Wichatitsky M, Ramirez B (2019) Vector-borne disease and climate change adaptation in African dryland social-ecological systems. Infect Dis Poverty 8:36.

[58] Mayo C, McDermott E, Kopanke J, Stenglein M, Lee J, Mathiason C, Perkins TA (2020) Ecological dynamics impacting bluetongue virus transmission in North America. Front Vet Sci 7:186.

[59] Sicuso DA, Previti A, Pugliese M, Passantino A (2025) Climate change impacts on livestock and resulting effects on animal health: current challenges in food safety, consumer protection, and animal welfare. J Consum Prot Food Saf 20:1–3.

[60] Elbers ARW, Koenraadt CJ, Meiswinkel R, Meiswinkel R (2015) Mosquitoes and Culicoides biting midges: vector range and the influence of climate change. Rev Sci Tech 34:123–137.

[61] Acevedo P, Ruiz-Fons F, Estrada R, Márquez AL, Miranda MA, Gortazar C, Lucientes J (2010) A broad assessment of factors determining Culicoides imicola abundance: modelling the present and forecasting its future in climate change scenarios. PLoS One 5:e14236.

[62] Malik AI, Ijaz M, Yaqub T, Márquez AL, Miranda MA, Gortazar C, Lucientes J (2018) Sero-epidemiology of bluetongue virus (BTV) infection in sheep and goats of Khyber Pakhtunkhwa province of Pakistan. Acta Trop 182:207–211.

[63] Liu F, Gong QL, Zhang R, Chen ZY, Wang Q, Sun YH, Du R (2021) Prevalence and risk factors of bluetongue virus infection in sheep and goats in China: a systematic review and meta-analysis. Microb Pathog 161:105170.

[64] Zhong J, Shu E, Zhang S, Yang Q, Chen Q, Niu B (2024) Prediction and transmission analysis of bluetongue disease in China. Prev Vet Med 230:106290.

[65] Xu W, Meng Z, Deng J, Sun X, Liu T, Tang Y, Zhu W (2022) Metabonomic identification of serum biomarkers related to heat stress tolerance of sheep. Anim Sci J 93:e13792.

[66] Shi LL, Wang ZQ, Xu YQ, Mao CY, Guo SW, Jin X, Shi BL (2020) Effects of heat stress on serum immune and antioxidative indexes and relative expression of related genes in sheep. Chin J Anim Nutr 32:5275–5284.

[67] Chauhan SS, Celi P, Leury BJ, Clarke IJ, Dunshea FR (2014) Dietary antioxidants at supranutritional doses improve oxidative status and reduce the negative effects of heat stress in sheep. J Anim Sci 92:3364–3374.

[68] Rebez EB, Sejian V, Silpa MV, Dunshea FR (2023) Heat stress and histopathological changes of vital organs: A novel approach to assess climate resilience in farm animals. Sustainability 15:1242.

[69] Bouzar AB, Boxus M, Florins A, François C, Reichert M, Willems L (2009) Reduced levels of reactive oxygen species correlate with inhibition of apoptosis, rise in thioredoxin expression and increased bovine leukemia virus proviral loads. Retrovirology 6:102.

[70] Liao Y, Tong L, Tang L, Wu S (2017) The role of cold-inducible RNA binding protein in cell stress response. Int J Cancer 141:2164–2173.

[71] Jeyachandran S, Chellapandian H, Park K, Kwak IS (2023) A review on the involvement of heat shock proteins (extrinsic chaperones) in response to stress conditions in aquatic organisms. Antioxidants 12:1444.

[72] Rouhiainen A, Kulesskaya N, Mennesson M, Misiewicz Z, Sipilä T, Sokolowska E, Hovatta I (2019) The bradykinin system in stress and anxiety in humans and mice. Sci Rep 9:19437. doi.org

[73] Borges TJ, Wieten L, Van Herwijnen MJ, Broere F, Van Der Zee R, Bonorino C, Van Eden W (2012) The anti-inflammatory mechanisms of Hsp70. Front Immunol 3:95.

[74] Romero RD, Montero Pardo A, Montaldo HH, Rodríguez AD, Hernández Cerón J (2013) Differences in body temperature, cell viability, and HSP-70 concentrations between Pelibuey and Suffolk sheep under heat stress. Trop Anim Health Prod 45:1691–1696.

[75] Naga AA, Khalek TA, Osman M, Elbeltagy AR, Abdel-Aal ES, Abou-Ammo FF, El-Shafie MH (2021) Physiological and genetic adaptation of desert sheep and goats to heat stress in the arid areas of Egypt. Small Ruminant Res 203:106499.

[76] Mohl BP, Roy P (2019) Hsp90 chaperones bluetongue virus proteins and prevents proteasomal degradation. J Virol 93:e00898-19. doi.org

[77] Dige MS, Gurao A, Mehrotra A, Singh MK, Kumar A, Kaushik R, Rout PK (2025) Comparative transcriptomic and co-expression network analysis identifies key gene modules involved in heat stress responses in goats. Int J Biol Macromol 305:140975.

[78] Chen N, Bai T, Wang S, Wang H, Wu Y, Liu Y, Zhu Z (2023) New insights into the role and therapeutic potential of heat shock protein 70 in bovine viral diarrhea virus infection. Microorganisms 11:1473.

[79] Alberti G, Paladino L, Vitale AM, Caruso Bavisotto C, Conway de Macario E, Campanella C, Marino Gammazza A (2021) Functions and therapeutic potential of extracellular hsp60, hsp70, and hsp90 in neuroinflammatory disorders. Appl Sci 11:736.

[80] Lubkowska A, Pluta W, Strońska A, Lalko A, Lalko A (2021) Role of heat shock proteins (HSP70 and HSP90) in viral infection. Int J Mol Sci 22:9366.

[81] Tenorio R, Fernández de Castro I, Knowlton JJ, Zamora PF, Sutherland DM, Risco C, Dermody TS (2019) Function, architecture, and biogenesis of reovirus replication neoorganelles. Viruses 11:288.

[82] Rojas JM, Avia M, Martín V, Sevilla N (2021) Inhibition of the IFN response by bluetongue virus: the story so far. Front Microbiol 12:692069.

[83] Dai M, Wang X, Li JL, Zhou Y, Sang M, Liu JB, Ho WZ (2015) Activation of TLR3/interferon signaling pathway by bluetongue virus results in HIV inhibition in macrophages. FASEB J 29:4978.

ISSN: **3107-6513**

[84] Au-Yeung N, Mandhana R, Horvath CM (2013) Transcriptional regulation by STAT1 and STAT2 in the interferon JAK-STAT pathway. Jak-stat 2:e23931.

[85] Blaszczyk K, Nowicka H, Kostyrko K, Antonczyk A, Wesoly J, Bluyssen HA (2016) The unique role of STAT2 in constitutive and IFN-induced transcription and antiviral responses. Cytokine Growth Factor Rev 29:71–81.

[86] Avia M, Rojas JM, Miorin L, Pascual E, Van Rijn PA, Martín V, Sevilla N (2019) Virus-induced autophagic degradation of STAT2 as a mechanism for interferon signaling blockade. EMBO Rep 20:e48766.

[87] Jiang H, Kan X, Ding C, Sun Y (2022) The multi-faceted role of autophagy during animal virus infection. Front Cell Infect Microbiol 12:858953.

[88] Tran DT, Batchu SN, Advani A, Advani A (2024) Interferons and interferon-related pathways in heart disease. Front Cardiovasc Med 11:1357343.

[89] Raftery N, Stevenson NJ (2017) Advances in anti-viral immune defence: revealing the importance of the IFN JAK/STAT pathway. Cell Mol Life Sci 74:2525–2535.